Effect of Series Resistances on Conversion Efficiency of GaAs/Si Tandem Solar Cells With Areal Current-Matching Technique

Masaaki Baba [ID], Kikuo Makita, Hidenori Mizuno, Hidetaka Takato, Takeyoshi Sugaya, and Noboru Yamada [ID], *Member, IEEE*

Abstract—The electrical losses due to the series resistances—the bonding resistance and sheet resistance—in a two-terminal (2T) GaAs/Si tandem solar cell that implements the areal current-matching (ACM) technique was investigated. A 2T GaAs/Si ACM tandem solar cell has a smaller top cell area and a larger bottom cell area, to achieve current matching between the top and bottom cells. The effect of the series resistances on the performance of such an ACM tandem cell was evaluated through device simulations, in which the subcell area ratio (bottom cell area / top cell area) and series resistances were varied under 1-sun and 3-sun conditions. The simulation results revealed that the optimal subcell area ratio at which the tandem cell exhibits the highest efficiency is affected mainly by the bonding resistance, due to a unique characteristic of the fill factor. A larger bonding resistance results in a smaller optimal subcell area ratio, i.e., a larger top cell area, which requires the use of a larger amount of expensive III–V materials. This trend is more prominent under 3-sun conditions. The indoor experiments conducted on an in-house 2T GaAs/Si ACM tandem cell verified the simulated results and showed that a lower external quantum efficiency (EQE) also resulted in a smaller optimal subcell area. Therefore, low bonding resistance and high EQE are of primary importance for realizing high-efficiency low-cost 2T ACM tandem solar cells.

Index Terms—III–V semiconductor materials, areal current matching, multijunction solar cell, silicon solar cells.

I. INTRODUCTION

S i-BASED III–V multijunction (MJ) solar cells have been attracting significant amounts of attention owing to their

M. Baba and N. Yamada are with the Department of Mechanical Engineering, Nagaoka University of Technology, Nagaoka 940-2188, Japan (e-mail: masaaki.bb@gmail.com; noboru@nagaokaut.ac.jp).

K. Makita and T. Sugaya are with the Research Center for Photovoltaics, National Institute of Advanced Industrial Science and Technology, Tsukuba 305-8568, Japan (e-mail: kikuo-makita@aist.go.jp; t.sugaya@aist.go.jp).

H. Mizuno and H. Takato are with the Renewable Energy Research Center, National Institute of Advanced Industrial Science and Technology, Koriyama 963-0298, Japan (e-mail: h-mizuno@aist.go.jp; h.takato@aist.go.jp).

Color versions of one or more of the figures in this paper are available online at http://ieeexplore.ieee.org.

cost effectiveness. The recorded maximum efficiency of a Si-based III–V MJ solar cell has exceeded 30% and thus has attracted attention as a next-generation high-efficiency low-cost solar cell [1]–[4]. The most common technology for fabricating Si-based III–V MJ solar cells is metamorphic epitaxial growth [5]–[11]. However, the following issues increase the difficulty of fabricating high-quality III–V MJ solar cells using epitaxial growth on a Si substrate: 1) Lattice mismatch and thermal expansion coefficient mismatch between Si substrates and III–V materials. 2) Defects such as antiphase domains generated by the difference in polarity between polar III–V materials and nonpolar Si crystals. Other approaches to fabricate Si-based III–V MJ solar cells include using mechanical stacking [12]–[16] and wafer bonding [2], [17]–[20]. The mechanical-stacking technique uses a transparent adhesive at the stacking interface. The GaInP/GaAs/Si triple-junction cell fabricated by wafer bonding currently demonstrates the highest cell conversion efficiency of 30.2% [2], although it requires chemical mechanical polishing to smooth the bonding surface with root-mean-square roughness values below 1 nm [21]. On the other hand, mechanical-stacking has been used frequently, owing to its simplicity. However, optical losses tend to be large owing to the opacity of the adhesive material and reflection at the junction interfaces. A smart stack [22], [23] is a mechanical stacking technique that uses metal nanoparticles instead of adhesives, and has less complicated processes, low optical losses, and high electrical conductivity.

Irrespective of the fabrication method, two-terminal (2T) MJ solar cells convert the sunlight energy at the highest efficiency when the current is matched in each of the subcells. However, in the structure of GaAs/Si tandem solar cells, if the GaAs absorbs all irradiation in the wavelength of the corresponding band gap, the Si bottom cell intrinsically limits the current under the AM1.5G solar spectrum because of the proximity bandgap of GaAs and Si, regardless of the fabrication method. The typical current-matching technique used to solve the current mismatch involves reducing the layer thickness of the top cell to allow a part of the light in the top cell bandgap pass through to the bottom cell. Recently, an alternative technique, the area current-matching technique (ACM) [13], has been proposed. In ACM, an MJ solar cell is composed of series-connected subcells that have different active cell areas; the areas of the subcells can be varied independently, to reduce the current mismatch. In case of

the GaAs/Si, the GaAs top cell area is smaller than the Si bottom cell. In principle, both techniques can achieve approximately the same efficiency under current matching conditions, based on the following assumptions.

1) There is no optical loss in the stacked area.
2) There is no electrical loss in the "extra" bottom cell area in the ACM technique.
3) The reflection loss at the top cell surface and "extra" bottom cell area surface is equal.

The main advantage of ACM is that it can reduce the top cell area in the current matching condition, consequently reducing the cost of the top cell per unit generated power. This advantage is more visible in solar cells that employ an expensive top cell and an inexpensive bottom cell, such as III–V/Si solar cells. Therefore, ACM has the potential to realize a cost-effective 2T III–V/Si MJ solar cell. A similar concept called the "step-cell" has also been introduced and a 2T GaAsP/Si tandem solar cell with a potential conversion efficiency of ∼26% has been demonstrated [24], [25]. In addition, a concept called "SMAC module" that combines the smart stack, ACM, and static low-concentration optics (nontracking) has been studied by the authors of this paper, who have reported that an SMAC module with 2T GaAs/Si tandem solar cells has the potential to achieve a conversion efficiency of ∼30% with lesser top cell area [22]. In the SMAC module, the concentration factor of the static concentrator optics is limited to ∼3 due to the acceptance angle limit of solar concentration.

When the ACM technique is applied to III–V/Si tandem solar cells, the bottom cell area must be larger than the top cell area; thus, the sheet resistance in the lateral direction of the bottom cell and the bonding resistance at the stacked interface are key factors that affect the electrical loss, i.e., the conversion efficiency. Until now, the effect of sheet resistance and bonding resistance, i.e., series resistances, on the conversion efficiency had not been discussed in detail under 1-sun and low-concentration (∼3-sun) conditions.

In this study, we characterized the effects of the series resistances in ACM 2T tandem solar cells (hereafter, termed as ACM solar cell) through device simulations and indoor experiments. The device simulations unveiled the theoretical effects of the series resistances on the ACM solar cell performance and optimal subcell area ratio. Furthermore, in order to verify the simulation results, a GaAs/Si ACM tandem solar cell was fabricated and tested for various active bottom cell areas, i.e., different subcell area ratios, under 1-sun and 3-sun conditions.

II. SIMULATION

To study the effect of series resistances on the ACM solar cell, the cell performances for various bottom cell areas were calculated through device simulations based on semiconductor physics [22], [26]. Fig. 1 shows the simulation model of an ACM solar cell. Equivalent circuit models of the top and bottom cells are connected in series. The bottom cell circuit has two components—a nonstacked area that receives sunlight directly and a stacked area—which are connected in parallel. The series resistances in the ACM solar cell, R_b and R_s, are defined
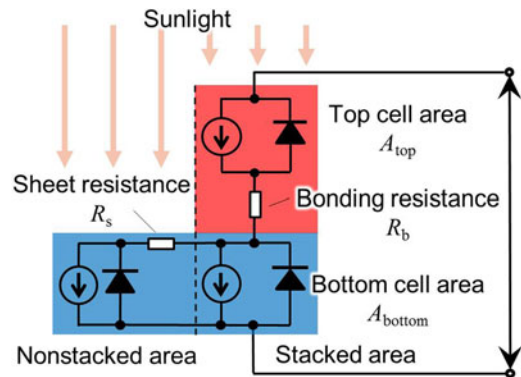

Fig. 1. Device simulation model for 2T ACM tandem solar cell. Note that A_{bottom} represents the entire bottom cell area including both nonstacked and stacked areas.
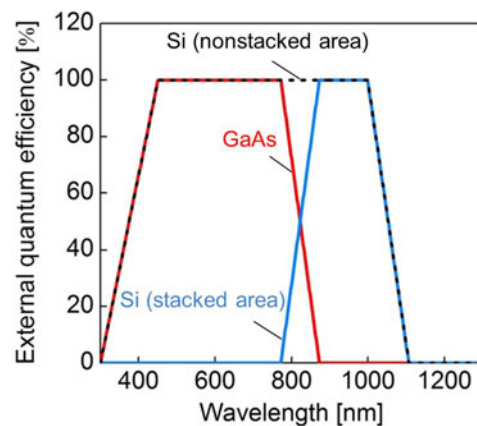

Fig. 2. External quantum efficiency model used for the simulation.

as the bonding resistance and sheet resistance, respectively. For simplicity, R_b and R_s are included in the top cell circuit and bottom cell circuit, respectively. The model consists of a constant top cell area A_{top} (0.16 cm^2) and variable bottom cell area A_{bottom} (0.16 − 0.27 cm^2). The lateral resistance of the bottom cell is calculated by sheet resistance and bottom cell area. The properties of the semiconductor materials of the Si solar cell used for the simulation, such as carrier lifetime, are the same as those reported in the literature [22]. The dark current density of GaAs used for simulation is 6×10^{-21} A/cm^2, which is the same as that reported by Alta Device [27]. Fig. 2 shows the external quantum efficiency (EQE) model of the top and bottom cells taken into account in the simulation. This EQE model reproduces the same short-circuit current density ratio of bottom cell to top cell for the subcell area ratio $A_{bottom}/A_{top} = 1$ as the measured value of the fabricated GaAs/Si tandem solar cell described in the next section, which is 0.45, i.e., the short-circuit current density of Si is approximately half of that of GaAs. The semiconductor device model used for the simulation is based on the following assumptions.

1) Bandgaps of GaAs and Si are 1.42 and 1.12 eV, respectively; the bottom cell limits the generated current under 1-sun standard test conditions (STC) when the subcell area ratio $A_{bottom}/A_{top} = 1$ (without ACM).

2) There is no loss of sunlight at the interface between the top cell and the bottom cell.
3) The cell temperature is 298.15 K.
4) The individual cell conversion efficiencies (under STC) of the GaAs top cell and Si bottom cell are 27.2% (short-circuit current density $J_{sc} = 27.5$ mA/cm^2, open-circuit voltage $V_{oc} = 1.1$ V, and fill factor FF = 0.89) and 20.7% ($J_{sc} = 39.9$ mA/cm^2, $V_{oc} = 0.62$ V, and FF = 0.83), respectively. The efficiency of the GaAs solar cell is close to the current record device efficiency [3], [27]. It should be noted that the efficiency of Si is ~6 percentage-points lower than the current record cell [28].

Fig. 3 shows the simulated solar cell performance (J_{sc}, V_{oc}, FF, and cell conversion efficiency η) for various R_b, R_s, and A_{bottom}/A_{top} ratios under 1-sun and 3-sun conditions. In Fig. 3(a), the J_{sc} curves show similar trends, regardless of the series resistances. Each J_{sc} curve has a peak value at a current-match area-ratio (CMAR), where the photogenerated currents of the top and bottom cells match. For $A_{bottom}/A_{top} \leq$ CMAR, J_{sc} increases as A_{bottom}/A_{top} increases, according to the following equation:

$$J_{sc} = \frac{\left(J_{sc\_bottom} - J_{sc\_top}\right) \times A_{top} + J_{sc\_bottom} \times \left(A_{bottom} - A_{top}\right)}{A_{bottom}}$$

$$= \frac{J_{sc\_bottom} \times A_{bottom} - J_{sc\_top} \times A_{top}}{A_{bottom}} \qquad (1)$$

where J_{sc_top} and J_{sc_bottom} represent the short-circuit current densities of the top cell and bottom cell, respectively. On the other hand, for $A_{bottom}/A_{top} \geq$ CMAR, J_{sc} decreases as A_{bottom}/A_{top} increases, according to the following equation:

$$J_{sc} = \frac{J_{sc\_top} \times A_{top}}{A_{bottom}}. \qquad (2)$$

In Fig. 3(b), the open-circuit voltage V_{oc} is nearly constant; it increases slightly by ~0.02 V, when the A_{bottom}/A_{top} ratio increases from 1.0 to 1.7, almost regardless of the series resistances. This increase in V_{oc} is due to the increase in sunlight absorption in the bottom cell. When the A_{bottom}/A_{top} ratio increases, the nonstacked area that receives full spectrum sunlight increases, thus the sunlight absorption in the bottom cell increases.

In Fig. 3(c), contrary to the J_{sc} curve trend, the FF curve shows a valley (minimum value) at CMAR and a higher value outside CMAR. The reason behind this trend is explained in Fig. 4, which shows the current–voltage curves of each subcell for $R_b = 5\,\Omega \cdot$ cm^2 and $R_s = 0\,\Omega$/sq. For $A_{bottom}/A_{top} = 1.0$, the bottom cell operates at its maximum power point. However, the top cell does not operate at its maximum power point, it operates at a point closer to the open-circuit point, where the gradient of the current–voltage curve is high, resulting in a high FF. In contrast, at $A_{bottom}/A_{top} = 1.38$ (CMAR), both subcells operate at the maximum power point, where the gradient of the current–voltage curve is low, resulting in the lowest FF. A similar trend has been observed in the conventional tandem solar cells with current mismatches due to spectral changes in the incident sunlight [29].
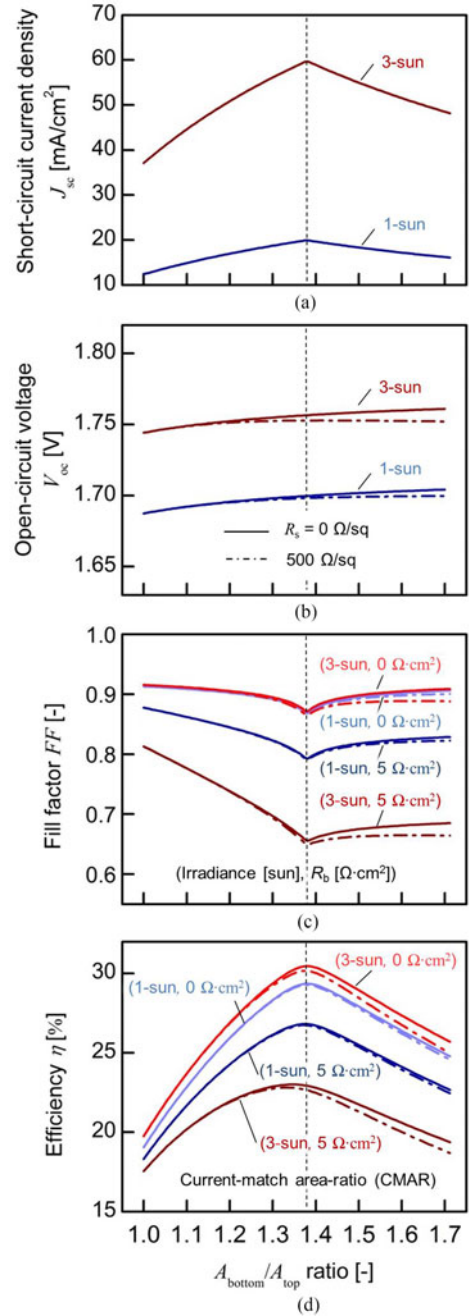

Fig. 3. Simulation results for 2T GaAs/Si ACM tandem solar cell. (a) Short-circuit current density, (b) open-circuit voltage, (c) fill factor, (d) cell efficiency when changing the bottom cell area, bonding resistance R_b, and sheet resistance R_s for a constant top cell area. In (c) and (d), the numbers in the brackets are the irradiance and bonding resistance.

Fig. 3(c) also shows that the absolute value of FF decreases and the negative gradient of FF in $1.0 < A_{bottom}/A_{top} <$ CMAR increases as R_b increases; this trend is emphasized under the 3-sun conditions. The effect of R_s on the FF characteristics is relatively lesser than that of R_b. Fig. 3(d) shows the resultant cell conversion efficiency η defined as the ratio of generated electricity to the incident sunlight power on the ACM solar cell area, which is equivalent to the entire bottom cell area. Since the open-circuit voltage is nearly constant, even when
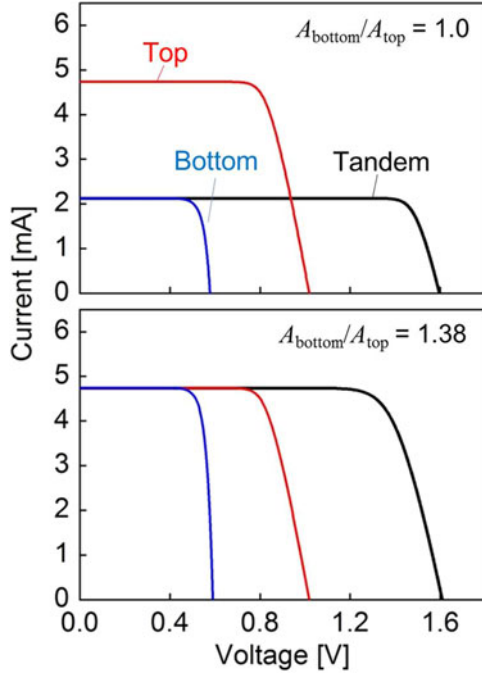
Fig. 4. Simulation results for 2T GaAs/Si ACM tandem solar cell. Current−voltage curves of each subcell and resultant current−voltage curves of tandem cell at $R_b = 5\,\Omega \cdot cm^2$ for $A_{bottom}/A_{top} = 1$ and 1.38 (CMAR) under 1-sun condition.
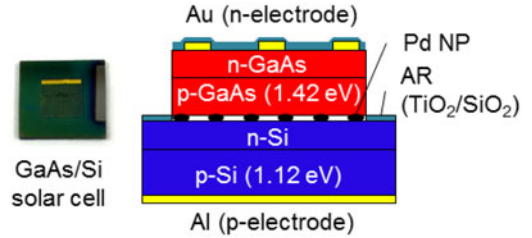

Fig. 5. Fabricated 2T GaAs/Si ACM tandem solar cell structure and cell dimensions.
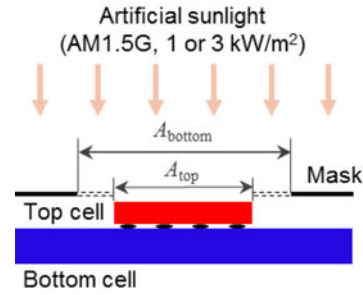

Fig. 6. Experimental setup to investigate the effect of $A_{bottom\_act}/A_{top\_act}$ ratio on solar cell performance. A_{bottom} was varied using masks with different unmasked areas. A_{top} was constant.

the A_{bottom}/A_{top} ratio varies, the efficiency will be proportional to FF $\times$ J_{sc}. As a result, each η curve has a peak at a certain A_{bottom}/A_{top}, i.e., the peak efficiency point (PEP).

The PEP appears near the CMAR, but not always exactly at the CMAR. When R_b and the irradiance increase, η decreases and the PEP shifts to a point slightly lower than the CMAR. Under 1-sun and $R_s = 0\,\Omega/sq$ conditions, PEP appears at $A_{bottom}/A_{top} = 1.381$ for $R_b = 0\,\Omega \cdot cm^2$, while PEP appears at $A_{bottom}/A_{top} = 1.375$ for $R_b = 5\,\Omega \cdot cm^2$; thus, the maximum η decreases by 2.54%abs from $R_b = 0$ to $5\,\Omega \cdot cm^2$. This trend is emphasized under the 3-sun conditions. PEP shifting to a lower A_{bottom}/A_{top} ratio is not desirable, because the smaller A_{bottom}/A_{top} ratio, the larger the area of the top cell will be, which will result in requiring expensive III–V materials.

These simulation results suggest that R_b remarkably affects the maximum value of η and the optimal A_{bottom}/A_{top} ratio of the ACM solar cell; thus, the reduction of R_b is of primary importance in the ACM solar cell.

III. EXPERIMENT

To verify the simulation results, indoor experiments were conducted. A 2T GaAs/Si ACM tandem solar cell was fabricated. Fig. 5 shows the cell structure of the fabricated solar cell. The dimensions of the electrode area of the top cell (A_E), top cell area (A_{top}), active top cell area ($A_{top\_act} = A_{top} - A_E$), and bottom cell area (A_{bottom}) are summarized in Fig. 5. The designed bandgaps of GaAs and Si were 1.42 and 1.12 eV, respectively, which were the same as those used in the simulation. The top and bottom cells were connected by palladium nanoparticles (Pd NP), both electrically and mechanically,

using the smart stack technique developed by AIST [23]. The measured individual cell efficiencies of the GaAs and Si subcells, which were measured before stacking, under STC were in the ranges of 16%–18% ($J_{sc} = 25\,mA/cm^2$, $V_{oc} = 0.9\,V$, $FF = 0.7 - 0.8$) and 13%–15% ($J_{sc} = 35\,mA/cm^2$, $V_{oc} = 0.6\,V$, $FF = 0.6 - 0.7$), respectively [20]. It is noted that the Si subcell efficiency was measured independently without a top cell. The efficiency of each subcell was ~10 percentage-points lower than that assumed in the simulation.

The sheet resistance of the Si bottom cell is mainly determined by the impurity concentration in the doped layer, and the measured sheet resistance of the nonstacked bottom cell area was 93 Ω/sq.

Fig. 6 shows the experimental setup. The fabricated solar cell performance was measured by changing the active bottom cell area $A_{bottom\_act} (= A_{bottom} - A_E)$ using masks with different unmasked areas. Here, the unmasked area is defined as A_{bottom}, and $A_{bottom\_act}/A_{top\_act}$ is used in the discussions instead of A_{bottom}/A_{top}. The cell temperature was controlled at 298.15 K by a cooling unit beneath the tested solar cell. The light source for the I–V measurement is a xenon lamp with an air mass filter. It should be noted that spectrum of the light source has a spectral mismatch in the near-infrared wavelength due to the bright line spectra of the xenon lamp.
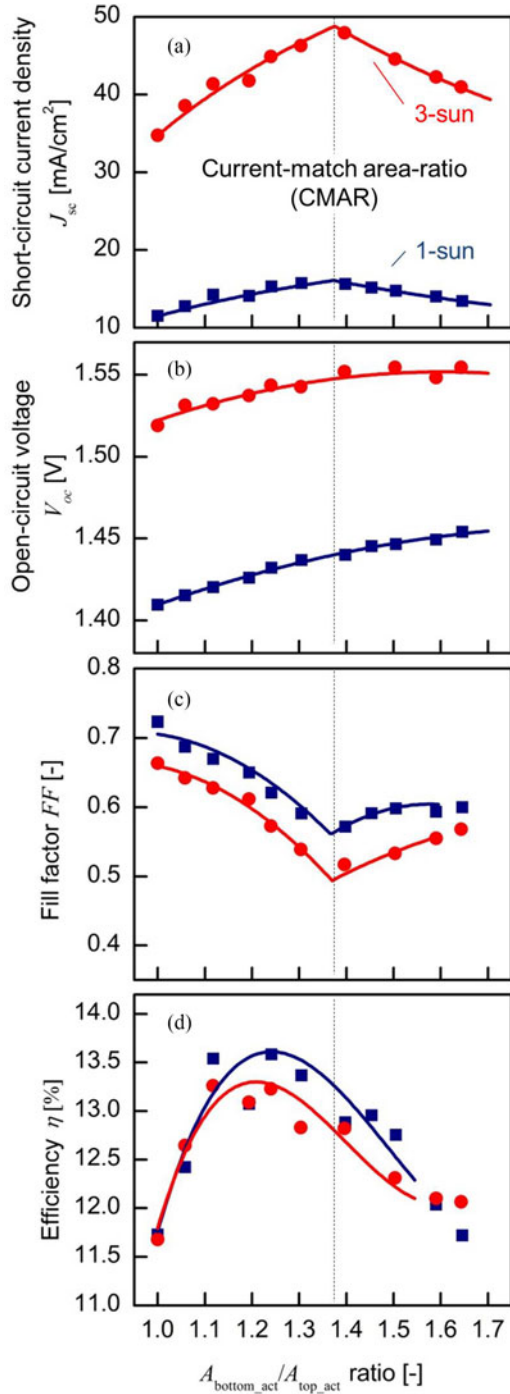
Fig. 7. Experimental results of the fabricated 2T GaAs/Si ACM tandem solar cell under 1-sun and 3-sun conditions. (a) Short-circuit current density, (b) open-circuit voltage, (c) fill factor, and (d) cell efficiency when changing the bottom cell area.
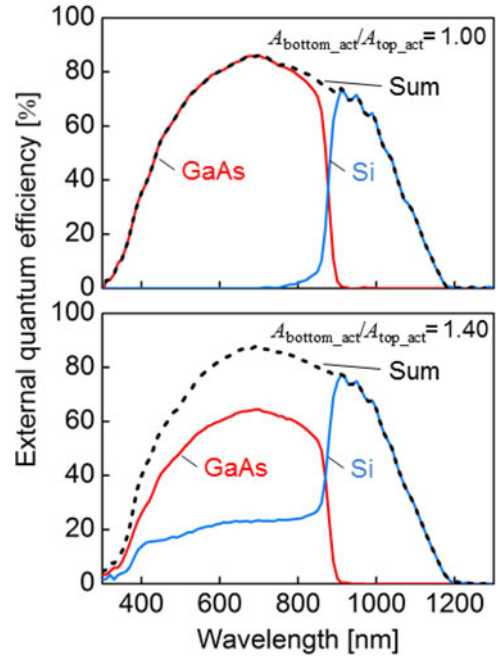

Fig. 8. Measured external quantum efficiency of the fabricated GaAs/Si tandem solar cell at $A_{\text{bottom\_act}}/A_{\text{top\_act}} = 1.00$ and 1.40 (closest to CMAR) conditions.

Fig. 7 shows the measured solar cell performances (J_{sc}, V_{oc}, FF, and η) under 1-sun and 3-sun conditions for various $A_{\text{bottom\_act}}/A_{\text{top\_act}}$, corresponding to Fig. 3. In Fig. 7(a), the measured J_{sc} were plotted with semitheoretical curves based on Eqs. (1) and (2), in which experimental values were input, e.g., measured short-circuit current at $A_{\text{bottom\_act}}/A_{\text{top\_act}} = 1.0$ for $(J_{\text{sc\_bottom}} - J_{\text{sc\_top}}) \times A_{\text{top}}$; measured short-circuit current

in the range of $A_{\text{bottom\_act}}/A_{\text{top\_act}} > \text{CMAR}$ for $J_{\text{sc\_top}} \times A_{\text{top}}$. Each J_{sc} curve had a peak at CMAR, which was consistent with the simulation result. The absolute value of the measured J_{sc} and gradient in $1.0 < A_{\text{bottom}}/A_{\text{top}} < \text{CMAR}$ were smaller than that of the simulated value due to real-world losses such as optical loss. Fig. 8 shows the measured EQE of the fabricated GaAs/Si tandem solar cell at $A_{\text{bottom\_act}}/A_{\text{top\_act}} = 1.00$ and 1.40 (closest to CMAR) conditions. The EQE of the fabricated cell was clearly lower than the EQE assumed in the simulation (Fig. 2).

To validate our simulation, we conducted the simulation again with the modified EQE model, which is more representative of the experimental device. Fig. 9(a) shows the modified EQE model, in which the maximum EQE is 80%. Fig. 9(b) shows the simulated J_{sc} in comparison with the measured J_{sc} [see Fig. 7(a)]. The simulated J_{sc} shows good agreement with the experimental results.

In Fig. 7(b), the measured V_{oc} also showed a result consistent with the simulation result, which increased slightly by 0.045 V, as $A_{\text{bottom\_act}}/A_{\text{top\_act}}$ increased from 1.0 to 1.65. This increment value of V_{oc} was approximately twice the simulation results due to a relative increase in the dark current at shading/masking parts of the bottom cell. The shading/masking parts lowered the V_{oc} level for every $A_{\text{bottom\_act}}/A_{\text{top\_act}}$ as compared with the simulation result.

In Fig. 7(c), the measured FFs are plotted along with the curves fitted by quadratic approximation. The approximated curves were obtained by assuming that each curve had a minimum value at each CMAR. The approximated curves fit well with the measured values although the measured points exhibited deviations from the approximated curve due to the
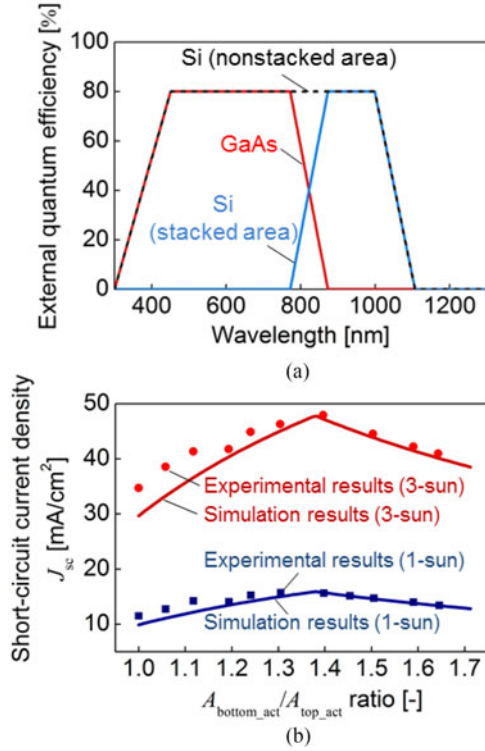
Fig. 9. Simulation results for 2T GaAs/Si tandem solar cell with modified EQE model. (a) Modified EQE model. (b) Simulated short-circuit current density.
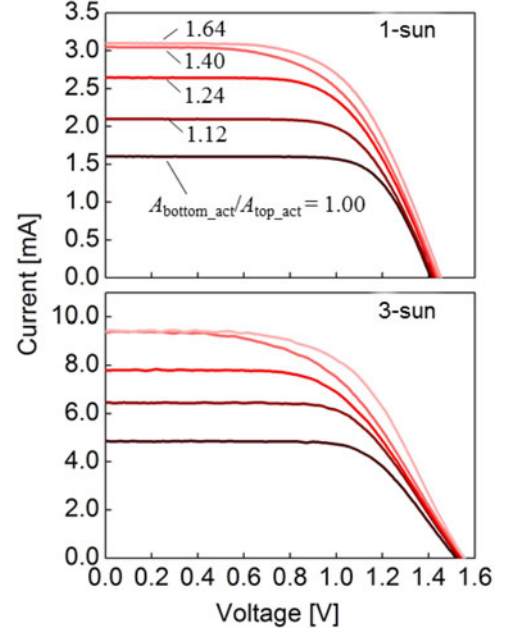

Fig. 10. Experimental results of the fabricated 2T GaAs/Si ACM tandem solar cell. Current-voltage curves of tandem cell for various $A_{bottom\_act}/A_{top\_act}$ under 1-sun and 3-sun conditions. $A_{bottom\_act}/A_{top\_act} = 1.40$ is the closest to CMAR.

sensitivity of the contact conditions between the measuring probe and the cell surface electrodes. The FF curves show trends similar to the simulated results, i.e., the FF curves exhibit a valley at CMAR and a higher value outside CMAR. Comparing Fig. 7(c) with the simulation results from Fig. 3(c), in the 1-sun condition, the rate of decline of FF in $1.0 < A_{bottom_act}/A_{top_act} < $ CMAR was higher than the simulation results of the $R_b = 5\,\Omega \cdot cm^2$ case, indicating that the series resistance of the fabricated solar cell was higher than $5\,\Omega \cdot cm^2$. In the 3-sun condition, the FF was lower than the 1-sun condition, and that trend was similar to the simulation. The measured R_s of the fabricated solar cell was approximately 1/5 of the $R_s = 500\,\Omega/sq$ assumed in the simulation, thus the effect of the R_s on FF was expected to be far less than that of R_b. The measured current–voltage curves are shown in Fig. 10, and they clearly show the decrease of FF at $A_{bottom\_act}/A_{top\_act} = 1.40$, which is the value closest to CMAR. The bonding resistance R_b estimated from the experiment was in the range of 5–8 Ω·cm.

In Fig. 7(d), the measured cell conversion efficiencies are plotted along with the curves fitted by cubic approximation. The PEPs of the efficiency curves for 1-sun and 3-sun conditions are $A_{bottom\_act}/A_{top\_act} = 1.24$ and 1.21, respectively, which are smaller than the CMAR. The reason why the measured efficiency curve shows an even smaller PEP than the simulated one is because the measured J_{sc} has a smaller gradient than the simulated one due to a lower EQE in the range of $1.0 < A_{bottom}/A_{top} < $ CMAR. The low FF of each subcell used in the experiment could also contribute to the shift of PEP.

It is confirmed that the simulation results are consistent with the experimental results. Increasing the EQE and bonding resistance are important for improving the efficiency and reducing the top cell area, which in turn reduces the use of III–V materials, which reduces the cost of the ACM solar cell. This importance increases in the cases where the ACM solar cell is used with increased solar concentration.

IV. CONCLUSION

The effect of the series resistances, i.e., the bonding resistance and sheet resistance, in 2T GaAs/Si tandem solar cells incorporated with the ACM technique was examined through device simulations and indoor experiments using an in-house solar cell. The simulation results showed that the fill factor and cell conversion efficiency decreased as the bonding resistance increased. The optimal subcell area ratio, which was a key design parameter of the ACM solar cell, was affected by the bonding resistance. A larger bonding resistance required a larger top cell area. Results of experiments conducted on an in-house ACM solar cell verified the simulation results and revealed the real-world effects, that is, a lower EQE also shifted the optimal subcell area ratio to be smaller, increasing the cell area of the III–V top cell relative to that of the Si bottom cell. These characteristics could be observed in ACM solar cells with other combinations of subcell materials in which the bottom is the current limiting subcell. It was noted that, in this study, the bonding resistance exerted a dominant effect on the cell performance compared with the sheet resistance, because the present cell size was small, i.e., in the scale of several millimeters; the decrease in cell performance due to sheet resistance could be more apparent in the case of a larger-sized cell. The fabricated 2T GaAs/Si ACM tandem cell showed worse performance than

the simulated result. In order to realize a higher efficiency of ~30%, improvement of the subcell performance, optimization of the antireflection coating, and reduction of the series resistances by improving the bonding process and electrode design are required. A possible method to reduce the series resistances would be applying a transparent oxide conductive layer to the stacked interface in the bonding process.

REFERENCES

[1] S. Essig *et al.*, "Raising the one-sun conversion efficiency of III–V/Si solar cells to 32.8% for two junctions and 35.9% for three junctions," *Nature Energy*, vol. 2, no. 9, 2017, Art. no. 17144.

[2] R. Cariou *et al.*, "Monolithic two-terminal III–V//Si triple-junction solar cells with 30.2% efficiency under 1-Sun AM1.5G," *IEEE J. Photovolt.*, vol. 7, no. 1, pp. 367–373, Jan. 2017.

[3] M. A. Green *et al.*, "Solar cell efficiency tables (version 50)," *Prog. Photovolt. Res. Appl.*, vol. 25, no. 7, pp. 668–676, 2017.

[4] N. Jain and M. K. Hudait, "III–V multijunction solar cell integration with silicon: Present status, challenges and future outlook," *Energy Harvesting Syst.*, vol. 1, nos. 3/4, pp. 121–145, 2014.

[5] Y. Buzynin *et al.*, "GaAs/Ge/Si epitaxial substrates: Development and characteristics," *AIP Adv.*, vol. 7, no. 1, 2017, Art. no. 015304.

[6] T. J. Grassman, D. J. Chmielewski, S. D. Carnevale, J. A. Carlin, and S. A. Ringel, "GaAs 0.75 P 0.25/Si dual-junction solar cells grown by MBE and MOCVD," *IEEE J. Photovolt.*, vol. 6, no. 1, pp. 326–331, Jan. 2016.

[7] K. N. Yaung, M. Vaisman, J. Lang, and M. L. Lee, "GaAsP solar cells on GaP/Si with low threading dislocation density," *Appl. Phys. Lett.*, vol. 109, no. 3, 2016, Art. no. 032107.

[8] L. Wang *et al.*, "GaAsP top solar cell of three-terminal GaAsP/SiGe on Si tandem solar cells," in *Proc. 29th Eur. Photovolt. Sol. Energy Conf. Exhib.*, 2014, pp. 2043–2045.

[9] B.-T. Tran *et al.*, "Fabrication and characterization of n-In0.4 Ga0.6 N/p-Si solar cell," *Sol. Energy Mater. Sol. Cells*, vol. 102, pp. 208–211, 2012.

[10] J. A. Carlin *et al.*, "High efficiency GaAs-on-Si solar cells with high Voc using graded GeSi buffers," in *Proc. 28th IEEE Photovolt. Spec. Conf.*, 2000, pp. 1006–1011.

[11] Y. Itoh, T. Nishioka, A. Yamamoto, and M. Yamaguchi, "14.5% conversion efficiency GaAs solar cell fabricated on Si substrates," *Appl. Phys. Lett.*, vol. 49, no. 23, pp. 1614–1616, 1986.

[12] S. Essig *et al.*, "Realization of GaInP/Si dual-junction solar cells with 29.8% 1-Sun efficiency," *IEEE J. Photovolt.*, vol. 6, no. 4, pp. 1012–1019, Jul. 2016.

[13] J. Yang, Z. Peng, D. Cheong, and R. Kleiman, "Fabrication of high-efficiency III-V on silicon multijunction solar cells by direct metal interconnect," *IEEE J. Photovolt.*, vol. 4, no. 4, pp. 1149–1155, Jul. 2014.

[14] H. Taguchi, T. Soga, and T. Jimbo, "Fabrication of GaAs/Si tandem solar cell by epitaxial lift-off technique," *Jpn. J. Appl. Phys.*, vol. 42, no. 12A, pp. L1419–L1421, 2003.

[15] Y. Yazawa *et al.*, "Three-junction solar cells comprised of a thin-film GaInP/GaAs tandem cell mechanically stacked on a Si cell," in *Proc. 26th IEEE Photovolt. Spec. Conf.*, 1997, pp. 899–902.

[16] J. M. Gee and G. F. Virshup, "A 31%-efficient GaAs/silicon mechanically stacked, multijunction concentrator solar cell," in *Proc. Conf. Rec. 20th IEEE Photovolt. Spec. Conf.*, 1988, pp. 754–758.

[17] A. C. Tamboli *et al.*, "III-V/Si wafer bonding using transparent, conductive oxide interlayers," *Appl. Phys. Lett.*, vol. 106, no. 26, 2015, Art. no. 263904.

[18] K. Tanabe, K. Watanabe, and Y. Arakawa, "III-V/Si hybrid photonic devices by direct fusion bonding," *Sci. Rep.*, vol. 2, p. 349, 2012.

[19] K. Tanabe, K. Watanabe, and Y. Arakawa, "1.3 μm InAs/GaAs quantum dot lasers on Si rib structures with current injection across direct-bonded GaAs/Si heterointerfaces," *Opt. Express*, vol. 20, no. 26, pp. B315–B321, 2012.

[20] P. Kopperschmidt, S. Senz, G. Kästner, D. Hesse, and U. M. Gösele, "Materials integration of gallium arsenide and silicon by wafer bonding," *Appl. Phys. Lett.*, vol. 72, no. 24, pp. 3181–3183, 1998.

[21] M. M. R. Howlader, P. R. Selvaganapathy, M. J. Deen, and T. Suga, "Nanobonding technology toward electronic, fluidic, and photonic systems integration," *IEEE J. Sel. Topics Quantum Electron.*, vol. 17, no. 3, pp. 689–703, May/Jun. 2011.

[22] M. Baba *et al.*, "Feasibility study of two-terminal tandem solar cells integrated with smart stack, areal current matching, and low concentration," *Prog. Photovolt. Res. Appl.*, vol. 25, no. 3, pp. 255–263, 2017.

[23] H. Mizuno, K. Makita, and K. Matsubara, "Electrical and optical interconnection for mechanically stacked multi-junction solar cells mediated by metal nanoparticle arrays," *Appl. Phys. Lett.*, vol. 101, 2012, Art. no. 191111.

[24] S. A. Hadi, E. A. Fitzgerald, and A. Nayfeh, "Theoretical efficiency limit for a two-terminal multi-junction 'step-cell' using detailed balance method," *J. Appl. Phys.*, vol. 119, no. 7, 2016, Art. no. 073104.

[25] S. A. Hadi, T. Milakovich, R. Shah, E. A. Fitzgerald, and A. Nayfeh, "Towards demonstration of GaAs0.76 P0.24/Si dual junction step-cell," in *Proc. 43rd IEEE Photovolt. Spec. Conf.*, 2016, pp. 1881–1886.

[26] S. M. Sze and K. K. Ng, *Physics of Semiconductor Devices*. Hoboken, NJ, USA: Wiley, 2006.

[27] "World's highest conversion efficiency of 26.33% achieved in a crystalline silicon solar cell," [Online]. Available: http://www.kaneka.co.jp/kaneka-e/images/topics/1473811995/1473811995_101.pdf.. Accessed on: May 14, 2017.

[28] B. M. Kayes *et al.*, "27.6% conversion efficiency, a new record for single-junction solar cells under 1 sun illumination," in *Proc. 37th IEEE Photovolt. Spec. Conf.*, 2011, pp. 4–8.

[29] A. Martí and A. Luque, Eds., *Next Generation Photovoltaics: High Efficiency Through Full Spectrum Utilization*. Bristol, U.K.: Inst. Phys. Publishing, 2004.

Authors' photographs and biographies not available at the time of publication.